

LC–MS/MS and chiroptical spectroscopic analyses of multidimensional metabolic systems of chiral thalidomide and its derivatives

Yoshiyuki Ogino¹  | Masahito Tanaka² | Togo Shimozawa¹  | Toru Asahi¹

¹Waseda University, Department of Life Science and Medical Bioscience, Tokyo, Japan

²National Institute of Advanced Industrial Science and Technology (AIST), Research Institute of Instrumentation Frontier, Tsukuba, Japan

Correspondence

Toru Asahi, Waseda University, Department of Life Science and Medical Bioscience, Tokyo, Japan.
Email: tasahi@waseda.jp

Funding Information

Grant-in-Aid for JSPS Fellows, Grant/Award Number: 14J07106

Abstract

Enantiomeric thalidomide undergoes various kinds of biotransformations including chiral inversion, hydrolysis, and enzymatic oxidation, which results in several metabolites, thereby adding to the complexity in the understanding of the nature of thalidomide. To decipher this complexity, we analyzed the multidimensional metabolic reaction networks of thalidomide and related molecules *in vitro*. Characteristic patterns in the amount of various metabolites of thalidomide and related molecules generated during a combination of chiral inversion, hydrolysis, and hydroxylation were observed using liquid chromatography–tandem mass spectrometry and chiroptical spectroscopy. We found that monosubstituted thalidomide derivatives exhibited different time-dependent metabolic patterns compared with thalidomide. We also revealed that monohydrolyzed and monohydroxylated metabolites of thalidomide were likely to generate mainly by a C-5 oxidation of thalidomide and subsequent ring opening of the hydroxylated metabolite. Since chirality was conserved in most of these metabolites during metabolism, they had the same chirality as that of nonmetabolized thalidomide. Our findings will contribute toward understanding the significant pharmacological effects of the multiple metabolites of thalidomide and its derivatives.

KEYWORDS

chiral inversion, chiroptical spectroscopy, enzymatic hydroxylation, hydrolysis, LC–MS/MS, thalidomide

1 | INTRODUCTION

The intricate molecular behavior of pharmaceutical products *in vitro* induced by hydrolysis, oxidation, reduction, conjugation, or isomerization leads to various pharmacological effects that may be consequential. These transformations could be beneficial or they could be harmful.^{1–3} Despite the structural transformations caused by developing drugs via metabolic actions including chiral inversion, which are of course thoroughly considered during *in silico* drug design, it is still difficult to predict all the effects of conformational isomers and stereoisomers of an active pharmaceutical

ingredient.^{4–6} Given the instability of drugs *in vitro*, not only the static discrimination of chirality is clinically important but the possibility of dynamic inversion at the stereogenic center must also be considered.^{7–9}

Thalidomide (TD)-induced teratogenicity, arguably the greatest drug disaster in history, underscores the importance of fugitive stereochemistry. The resident (*S*)-isomer of orally prescribed TD was identified as the principle cause of the adverse reaction, whereas the (*R*)-isomer exhibited a prescriptive sedative hypnotic effect.¹⁰ However, because of the high acidity of the stereocenter hydrogen atom of the glutarimide ring, TD undergoes

facile chiral inversion under physiological pH and temperature conditions.^{11,12} This isomerization is accompanied by nonenzymatic hydrolysis and enzymatic hydroxylation *in vivo*, prompting our interest in the toxicity of its metabolites. Some of the ring-opened hydrolytic products were reported to be a more potent inhibitor of tumor necrosis factor- α (TNF- α) production than unmetabolized TD.^{13,14} Another report theoretically proposed the mechanism that TD or its ring-opened products selectively bind to specific consensus sequences, GC boxes, and suppressed the expression of some proteins relating to limb growth.¹⁵ Previous animal examinations revealed that various mono- and dihydroxylated TD metabolites are formed in the presence of CYP450, mainly 2C19, involved in the liver microsome, and exhibit an enhanced efficacy for the antiinflammatory effect compared with unmetabolized TD.¹⁶⁻¹⁹ In particular, oxidation of TD occurring at the C-5' position in the glutarimide ring induces a new stereoisomerism. Oxidation of TD occurring in the phthalimide ring leads to further hepatic metabolic reactions such as glutathione conjugation and glucuronic acid conjugation.²⁰⁻²² Thus, TD has multiple reaction sites for hydrolysis and hydroxylation and several metabolic products of TD and their enantiomers have been identified with experimental analyses (Figure 1A, Figures S1, S2).

Multiple functions and behaviors relevant to TD have already been identified in previous studies. It has been suggested that the intercalation of TD into stacked intracellular DNA basepairs via the plane structure of its phthalimide ring induces DNA oxidation, which may trigger an anticancer effect.¹⁵ We previously demonstrated that TD and a fluorinated derivative, 3'-fluorothalidomide (3'-FTD), show self-disproportionation of enantiomers, which may lead to an enantiospecific function of TD against racemization.^{23,24} Recently, cereblon (CRBN) has been identified as a TD target protein for suppressing the production of growth factor FGF8 during the organogenesis stage and inducing malformation or total absence of a fetal limb.²⁵⁻²⁷ Structural studies of CRBN and the binding molecules have been reported recently, and revealed the structural characteristics of the potential moiety of TD and its derivatives that bind to the target proteins and evoke translational signaling cascades.^{28,29} The medicinal properties of TD such as its hypnotic, sedative, and teratogenic effects seem to result from these multiple effects, which are still indeterminate. Furthermore, several derivatives and analogs of TD have been developed to reduce its side effects and other properties such as its slow chiral inversion.^{22,30-37} However, it is uncertain whether the existence of various structures including TD, its derivatives, and their metabolites is the

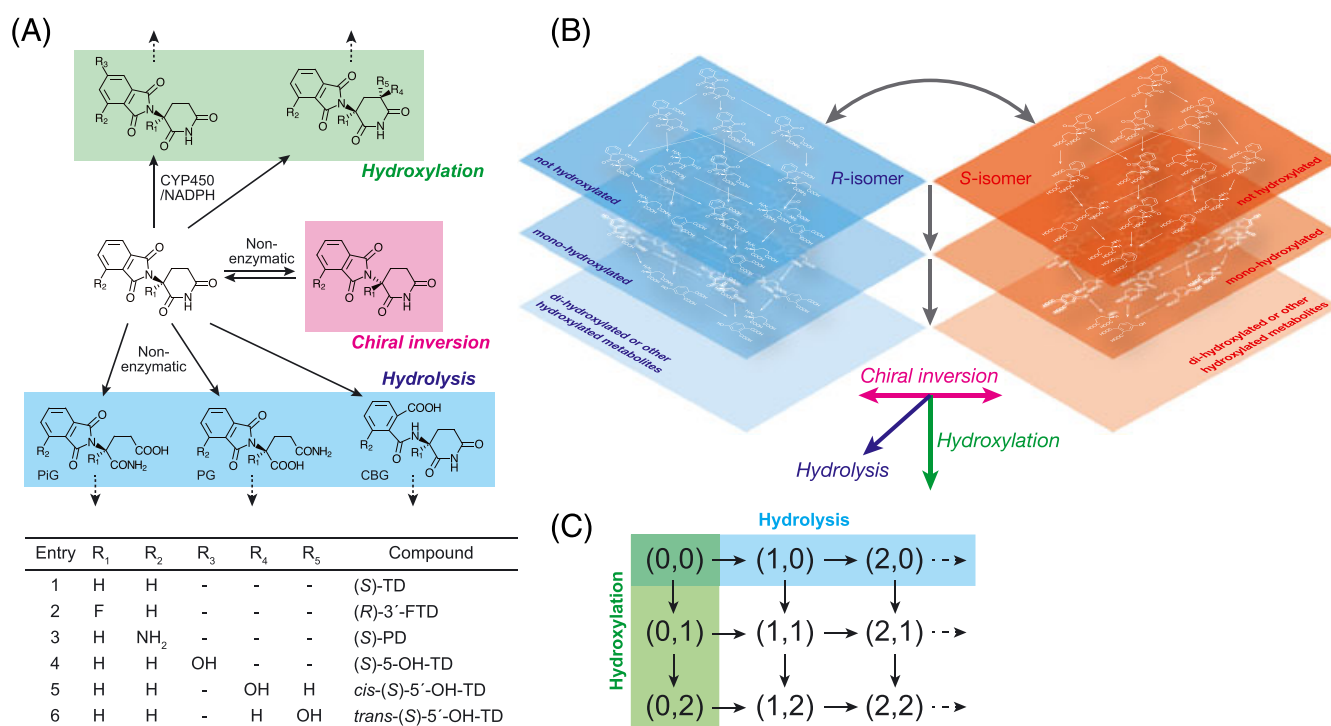


FIGURE 1 (A) Biotransformation pathways of enantiomeric TD involving nonenzymatic chiral inversion, hydrolysis, and enzymatic hydroxylation. Different combinations of substituents R_{*i*} (*i* = 1, 2, 3, 4, 5) on TD determines different derivatives and structural isomers of mono-hydroxylated metabolites. (B) Schematic of three-directional and hierarchical metabolic reaction network of TD. TD undergoes hydrolysis on the illustrated location and suffers from chiral inversion as indicated by the mirrored plane. Oxidation of TD is demonstrated by moving downward in the layers. (C) The definitions of (*i,j*)-metabolites in the present study

reason why TD is effective for various intractable diseases. We consider that this struggle stems from the complexity of the metabolic reaction pathways of TD, which includes spontaneous hydrolysis and chiral inversion, as well as enzymatic hydroxylation (Figure 1B). In our computational approaches toward understanding of the complexity of TD metabolic reaction pathways, we quantitatively simulated the temporal changes in the concentration and the enantiomeric excess of hydrolytic metabolites of TD during spontaneous chiral inversion and hydrolysis by using experimental and theoretical kinetic parameters for TD metabolism.³⁸ This study enabled us to expansively comprehend the molecular biological assays analyzing the antiinflammatory effects of TD hydrolytic metabolites from the viewpoint of the dynamic metabolism of TD. Since the metabolic reaction network of TD has not been achieved, the preferred metabolic pathway is not understood.

In this study, we experimentally analyze the progress of the metabolic reaction network of chiral TD by employing liquid chromatography–tandem mass spectrometry (LC–MS/MS) and chiroptical spectroscopy. The metabolism of TD derivatives such as 3'-FTD and TD amino derivatives of TD, pomalidomide (PD), are also examined to reveal the structural effects of substituents on the TD molecule on the progress of the metabolic reaction network. Furthermore, we monitor the changes in the chirality of hydrolyzed and hydroxylated metabolites by measuring the temporal changes in the circular dichroism (CD) spectra during the metabolic reactions. To estimate the preferred metabolic pathway of the multiple possible pathways, we calculate the energy barriers for the first hydrolysis step of TD and hydroxylated TD into their glutarimide ring-broken products by using density functional theory calculations.

2 | MATERIALS AND METHODS

2.1 | Chemicals

(*R*)-(+)-, (*S*)-(–)-, and (*RS*)-TD were synthesized as previously described. The hydrolytic products of TD, (*S*)- and (*RS*)-phthaloylisoglutamine (PiG), (*S*)- and (*RS*)-phthaloylglutamine (PG), and (*S*)- and (*RS*)-2-(α -carboxybenzamide) glutarimide (CBG), were purchased from Tokyo Chemical Industry Co., Ltd. (Japan). Racemic 3'-FTD was synthesized as previously reported. Racemic PD was purchased from Sigma-Aldrich (Japan). All other chemicals used in the present study to dissolve chemical compounds were all of spectroscopic analytical grade and purchased from Wako Pure Chemical Industries, Ltd. (Japan). Ethyl-*p*-hydroxybenzoate, which was used as an internal standard for LC–MS/MS, was also purchased from Wako Pure Chemical Industries, Ltd. (Japan).

2.2 | Hydrolysis of TD and its derivatives

In this study, hydrolysis of the samples was performed before hydroxylation of the samples. Enantiomeric and racemic TD, 3'-FTD, and PD were dissolved in dimethyl sulfoxide (DMSO) (10 mM). The highly concentrated solutions were then mixed with 100 times volume of 0.1 M potassium phosphate buffer (pH 7.4). The mixture (total volume of 500 μ L) was incubated at 37 °C for 1, 2, and 3 h. To avoid the influence on the function of oxidation enzymes by using organic solvents to stop the reaction, hydrolysis was instead terminated by rapid freezing of the reaction solution. These samples were stored at –80 °C.

2.3 | Hydroxylation of TD and its derivatives

Hydroxylation reactions were performed with a typical incubation mixture (total volume of 200 μ L) containing 0.1 mM EDTA (Dojindo, Japan), an NADPH-generating system (1.3 mM NADP⁺ (Oriental Yeast, Japan), 3.3 mM glucose 6-phosphate (Wako), 0.4 unit mL^{–1} glucose 6-phosphate dehydrogenase (Oriental Yeast) and 3.3 mM MgCl₂ (Wako)), CD-1 mouse liver microsomal extract (protein content \geq 20 mg mL^{–1}) (Sigma-Aldrich, Japan), and the hydrolyzed samples (100 μ M). To stop unnecessary degradation of TD, 3'-FTD, and PD via hydrolysis, all the above-mentioned procedures were carried out quickly and on ice. Each resulting mixture was then incubated at 37 °C for 10, 30, and 60 min. Incubation was terminated by adding 200 μ L of ice-cold CH₃CN. The internal standard (ethyl-*p*-hydroxybenzoate) was added into the sample solutions at a final concentration of 100 μ M. The solutions were centrifuged at 1700 *g* at 4 °C for 15 min, and then collected separately into an organic supernatant. These samples were filtrated with a spinfilter (Merckmillipore, Japan) and the StrataX solid-phase extract cartridge with polymer stationary phase (Shimadzu, Japan). These samples were then applied on LC–MS/MS systems and a circular dichroism spectropolarimeter to obtain absorbance and CD spectra.

2.4 | LC–MS/MS assays

LC–MS/MS analyses of the complex metabolic reaction network of TD and its derivatives were performed on a Shimadzu Prominence HPLC system connected to an AB SCIEX TripleTOF system mass spectrometer (AB SCIEX, Japan). TD, 3'-FTD, PD, as well as their early-stage metabolites, were analyzed in the mass spectrometer (MS) positive ion mode. Liquid chromatography conditions were as follows: buffer A contained 0.1% HCOOH (v/v) in 5% CH₃CN and 95% H₂O (v/v), and buffer B contained 0.1% HCOOH (v/v) in 95% CH₃CN and 5% H₂O (v/v). The gradient program used in these analyses with a flow rate of

0.2 mL min⁻¹ was as follows: 0 to 1 min, hold at 99% A, 1 to 3 min, linear gradient from 99% A to 1% A (v/v), 3 to 5 min, hold at 1% A, 5 to 6 min, linear gradient from 1% A to 99% A (v/v), 6 to 10 min, hold at 99% A. The column temperature was set at 25 °C with a column oven. The prepared samples (5 µL) were infused with an autosampler. MS analyses were carried out in the ESI-TOF positive ion mode. Total ion chromatograms of the metabolites of TD and its derivatives were acquired over the range *m/z* 100–1000 with a Shiseido CAPCELL CORE ADME adamantyl semimicro column (2.1 × 100 mm). The *m/z* of the fragment ions of metabolites of TD and its derivatives were also obtained over the range *m/z* 100–300. ESI conditions were as follows: capillary voltage, 2.5 V; sampling cone, 30; extraction cone, 4.1; source temperature, 120 °C; desolvation temperature, 325 °C; and Trap CE parameter, 6. Hydrolyzed and hydroxylated metabolites of TD, 3'-FTD, and PD were quantified by the peak area of extracted ion chromatogram (XIC) at the monoisometric exact mass displayed in Table S1 (mass tolerance: ±0.1 Da). For quantification of each metabolite, the proper *m/z* transitions during MS/MS fragmentation were employed because of the lack of an authentic standard, such as the *m/z* 293 → 225 transition of (1,1)-metabolites (Figure S3). The XICs of the internal standard were utilized to verify adequate ionization of the sample. The XICs of these *m/z* were acquired using the AB SCIEX Analyst TF 1.7 software.

2.5 | Circular dichroism spectroscopy

Hydrolyzed and hydroxylated samples (~200 µL) were diluted with the same volume of diluted water. CD and absorbance spectra were measured using a J-820 CD spectropolarimeter (Jasco, Japan) with a quartz cell under the following conditions: scan speed, 100 nm min⁻¹; temperature of the cell holder, 27 °C (using a Peltier device cell holder); sensitivity, standard (100 mdeg). Blank tests for CD and absorbance spectra were performed with a 1:1 mixture of diluted water and CH₃CN.

2.6 | Data analysis

The generated metabolites of TD, 3'-FTD and PD were quantified from the peak areas of XIC for the specified *m/z* of each metabolite listed in Table S1. Absolute values of the area of peak at retention time (*t_R*) were calculated using the Origin 2016 software (LightStone, Japan). All graphs displayed in the present study were also drawn using Origin 2016 software.

2.7 | Geometrical optimization

All quantum chemical calculations in the present study, including structure optimization and electron transition calculations, were performed using Gaussian09 (Revision D.01) and GaussView5.³⁹ The initial coordinates of enantiomeric and racemic TD and racemic 3'-FTD were obtained from their crystal structure, which we previously reported.^{23,40} The initial structure of racemic PD was acquired by the modification of the crystal structure of racemic TD. The initial structure of one of the first-generation hydrolytic products, (*S*)-CBG, was acquired from the crystal structure obtained by our X-ray crystallographic analysis (unpublished). The B3LYP/6–311+g(d,p) basis set was used for geometrical optimization of the substrate and the first-generation hydrolytic products of TD, 3'-FTD, and PD.

2.8 | Computation of absorbance and CD intensity

Theoretical CD and absorbance intensities were obtained by calculating the transition intensities and rotatory strengths of each singlet excitation at the B3LYP/6–311+g(d,p) level of theory for 5-hydroxylated TD (5-OH-TD), *cis/trans*-5'-hydroxylated TD (*cis/trans*-5'-OH-TD), 5-hydroxylated CBG (5-OH-CBG), and *cis/trans*-5'-hydroxylated CBG (*cis/trans*-5'-OH-CBG).

2.9 | Calculation of activation energy of metabolic reactions

To estimate the activation energy for hydrolysis of TD into CBG, the structure of the transition state (TS) was determined. The activation energy was calculated as the difference between the electron energy of the TS structure and that of the substrate structures (TD + H₂O). The substrate structures were optimized using the B3LYP/6–311+g(d,p) basis set. To reveal the effect of oxidation on TD, we also calculated the activation energy for the reactions of 5OH-TD, *cis*-5'-OH-TD, and *trans*-5'-OH-TD into 5OH-CBG, *cis*-5'-OH-CBG, and *trans*-5'-OH-CBG. These substrate structures were also optimized using the same level of computations.

3 | RESULTS AND DISCUSSION

3.1 | Multiple steps of hydrolysis and hydroxylation

We first defined the group of metabolites that suffered from *i*-times hydrolysis and *j*-times hydroxylation as (*i,j*) (unmetabolized molecule can be written as (0,0)). Hydrolysis, hydroxylation, and chiral inversion are then expressed as (*i,j*) → (*i* + 1,*j*), (*i,j*) → (*i,j* + 1), and

(R)-(*i,j*) \rightleftharpoons (S)-(*i,j*), respectively (Figure 1C). Note that some of the hydrolysis reactions increase the mass of metabolites by ~ 1 Da, which is not caused by the addition of a hydrogen atom but the replacement of an amino moiety with a hydroxyl moiety (Table S1).

To consider the initial relationship between hydrolysis and hydroxylation initially, we let TD undergo spontaneous hydrolysis and enzyme-driven hydroxylation with the different reaction times for hydrolysis (1–3 h) and hydroxylation (10–60 min). We detected various metabolites suffering from multiple times of hydrolysis and hydroxylation. In the present study we focused on the upstream major four metabolites including unmetabolized TD. Figure 2A shows the XICs at

m/z 259.07, 275.06, 277.08, and 293.08 of the sample with 1 h of hydrolysis and 30 min of hydroxylation of (S)-TD. We plotted the time dependence of the amount of unmetabolized TD (0,0), and other hydrolyzed and hydroxylated metabolites (*i,j*) for $i = 0, 1$ and $j = 0, 1$ (Figure 2B). The areas of peak at $t_R = 4.80$ for TD, $t_R = 1.12$ for (0,1)-metabolites, $t_R = 4.32$ for (1,0)-metabolites, and $t_R = 1.55$ for (1,1)-metabolites were utilized to draw the level plots. We acquired the unique metabolic patterns for the principal metabolites of TD. In the timescale of the metabolic reactions employed in the present study, TD hydrolysis seems to mainly proceed in the first step hydrolysis, TD into PiG, PG, and CBG. In accordance with the preceding report that

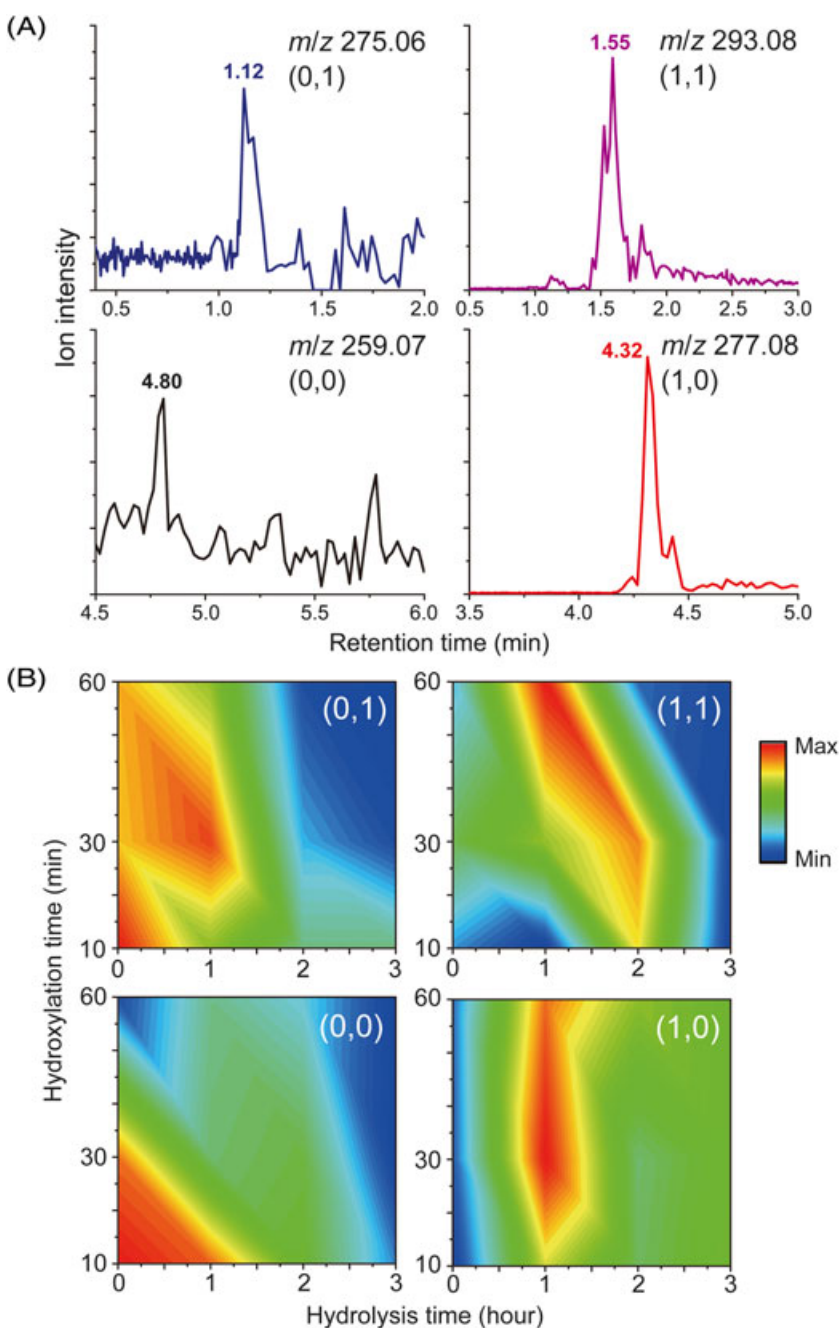


FIGURE 2 (A) XICs at m/z 259.07 for (0,0)-metabolite (TD), m/z 275.06 for (0,1)-metabolites, m/z 277.08 for (1,0)-metabolites, and m/z 293.08 for (1,1)-metabolites of the sample with 1 h of hydrolysis and 30 min of hydroxylation of (S)-TD. (B) Level plots of the amount of (0,0), (0,1), (1,0), and (1,1)-metabolites for different hydrolysis and hydroxylation reaction times of (S)-TD. The plots were obtained from the peak areas of XICs such as presented in (A) with different metabolic reaction times. The amounts of metabolites were normalized to the maximum amount of each metabolite

(1,0)-metabolites are rather stable against further degradation, few (2,0)- and other downstream metabolites are generated during this timescale.¹³ Therefore, the generation and degradation of (1,1)-metabolites seem to occupy an important part of the metabolic reaction network. As hydrolysis and hydroxylation proceeded, the amount of TD showed a rapid decrease, resulting in the formation of downstream metabolites including (1,0)- and (0,1)-metabolites along with both the reaction time of hydrolysis and hydroxylation. Meanwhile, (1,1)-metabolites were formed gradually as hydrolysis and hydroxylation of TD proceeded. The amount of (1,1)-metabolites reached a maximum within 1 h of hydrolysis and 60 min of hydroxylation. Note that TD hydrolysis can also occur during the hydroxylation reaction time since TD is exposed to the aqueous buffer during the enzymatic hydroxylation. Therefore, the hydroxylation reaction time also encompasses hydrolysis. Following a maximum, the (1,1)-metabolites seemed to degrade into the downstream metabolites owing to subsequent reactions. This suggests that the relationship between hydrolysis and hydroxylation produces a characteristic metabolic pattern on each metabolic layer and affects the whole system of layered metabolic reactions.

3.2 | Preferred pathway in temporal formation of monohydroxylated TD metabolites

Next, we focused on the monohydrolyzed and monohydroxylated metabolites of TD, i.e., (1,1)-metabolites. Our experimental results revealed that certain hydrolysis and hydroxylation reaction times are needed to generate (1,1)-metabolites. During the production of (1,1)-metabolites, the following three pathways are possible (Figure 3A): 1) TD

degrades into (1,0)-metabolites, after which the (1,0)-metabolites suffer from hydroxylation mainly at C-5 on the phthalimide ring or C-5' on the glutarimide ring resulting in (1,1)-metabolites; 2) TD undergoes hydroxylation at C-5 first, and then, (0,1)-metabolites suffer from hydrolysis resulting in (1,1)-metabolites; and 3) TD undergoes hydroxylation at C-5' first, and then, the (0,1)-metabolites suffer from hydrolysis resulting in (1,1)-metabolites. Note that other oxidations of TD rings such as at C-4 or at the nitrogen atom in the glutarimide ring can also occur. In the present study, however, we focused on C-5 and C-5' oxidation of TD because the other hydroxylated metabolites are not dominant during TD metabolism.^{17,18}

To consider these three preferred pathways, we examined whether (1,0)-metabolites of TD are hydroxylated in the presence of oxidation enzymes. Figure 3B illustrates the XICs at m/z 293.08 of the hydroxylation samples of TD and the most abundant (1,0)-metabolites, CBG. Compared with the XIC of the sample generated from TD, small ion intensities were observed at the XICs of the samples generated from CBG. We then measured the amount of (1,1)-metabolites generated from TD and CBG using the obtained peak area of the XICs (Figure 3C). Note that the concentrations of each substrate TD and CBG were set to the same in Figure 3B. Since part of TD was only converted to (1,0)-metabolites after 1 h of hydrolysis, the amount of (1,1)-metabolites generated from TD should be smaller than that generated from CBG. However, the amount of (1,1)-metabolites generated from CBG was small compared with that generated from TD with experimental replications. Therefore, we found that (1,0)-metabolites of TD were less likely to suffer from enzymatic hydroxylation. Other (1,0)-metabolites were also oxidized into (1,1)-metabolites, which can be negligible

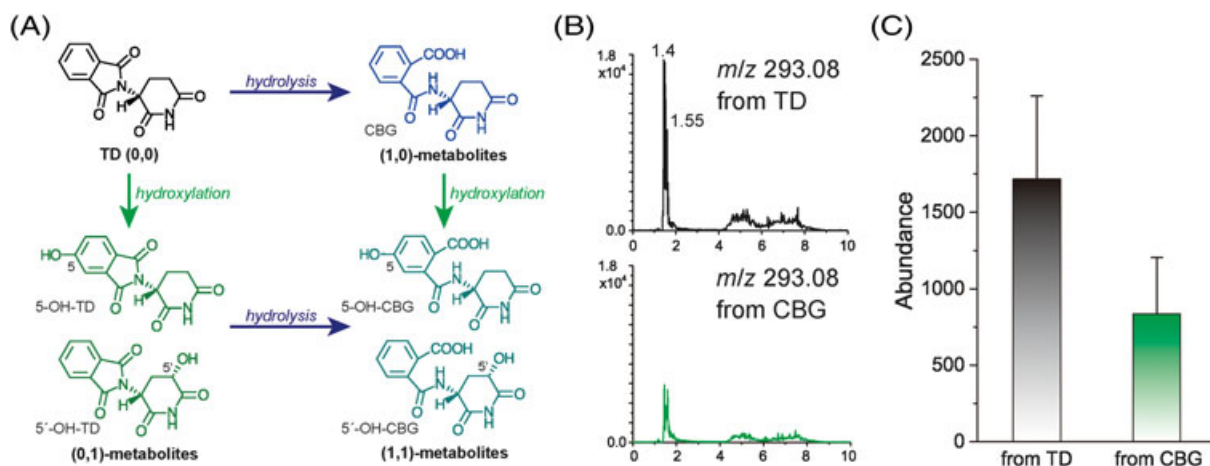


FIGURE 3 (A) Possible metabolic pathways of the formation of (1,1)-metabolites involving hydrolysis and hydroxylation. In this figure, the pathway relevant to CBG was chosen to represent (1,0)-metabolites because CBG is the most abundant metabolite among (1,0)-metabolites of TD. (B) XICs at m/z 293.08 representing the amount of (1,1)-metabolites generated from TD and CBG. (C) The amount of (1,1)-metabolites generated from TD and (1,0)-metabolites after 1 h of hydrolysis and 60 min of hydroxylation (TD) and after 60 min of hydroxylation (CBG). The values represent mean values ($n = 3$) \pm standard deviation

due to the small presence of PiG and PG during metabolism (Figure S4).¹³ The stability of (1,0)-metabolites during hydroxylation also supports our conclusion. Further, the hydrolysis rate constant of 5-OH-TD has previously been reported to be relatively smaller than that of unmetabolized TD, whereas that of 5'-OH-TD is almost the same as that of unmetabolized TD.⁴¹ Our experiments and the results described in Yamamoto et al.⁴¹ lead us to choose pathway (3) as a major pathway. According to these analyses, ring opening of TD and oxidation at C-5 on the phthalimide ring possibly inhibit subsequent hydroxylation and hydrolysis, respectively. This implies that these properties relevant to microscopic chemical reactions on each metabolite play an important role in determining the hierarchy of the metabolic reactions.

3.3 | Substituent effect on the temporal di-hydroxylation

Although the hydrolysis rate constants of 3'-FTD and PD differ from those of TD, they show almost the same behavior as TD. To examine the effect of the substituent on the TD molecule on the metabolic character, we next plotted the time-dependent formation of di-hydroxylated metabolites of TD, 3'-FTD, and PD with different hydrolysis and hydroxylation reaction times (Figure 4). To understand the progress of the metabolic reaction network in terms of the metabolic layer, we did not discriminate between the structural isomers of di-hydroxylated metabolites, which we regarded as belonging to the same metabolic layer, i.e., (0,2)-metabolites.

In these plots, the peak areas of XICs at m/z 291.06 for (0,2)-metabolites of TD, m/z 309.05 for (0,2)-metabolites of 3'-FTD, and m/z 306.07 for (0,2)-metabolites of PD were normalized by the maximum value of the peak areas. Di-hydroxylated metabolites were generated gradually after around 30 min of hydroxylation, but degraded with increased hydroxylation reaction time owing to the ring breakdown of hydroxylated TD. For 3'-FTD and PD, the amount of (0,2)-metabolites reached a maximum with 30 min of hydroxylation and without any hydrolysis reaction time, whereas for TD, (0,2)-metabolites reached their maximum after 60 min of hydroxylation and with a short hydrolysis reaction time. This indicates that substitution of fluorine at the stereogenic center causes the acceleration of P450-driven hydroxylation. The fluorine atom substituted at the stereogenic center acts as an electron-withdrawing moiety and affects the electron density of 3'-FTD. The slight mesomeric effect of the fluorine atom might also contribute to the rapid hydrolysis as well as acceleration of hydroxylation. Amino moiety substitution on the aromatic/nonaromatic ring structures seems to have almost the same effect as the fluorine atom.

Figure 4A shows that di-hydroxylation of TD requires some hydrolysis time, which seems to be usually unnecessary for oxidation of substrate. Chowdhury et al. previously reported a nonenzymatic oxidation pathway of 5-hydroxylated TD.²⁰ In their hypothesis, an intermediate of the addition of a water molecule to 5-OH-TD can be formed during keto-enol tautomerism in 5-OH-TD evoked by electron transfer from the hydroxyl moiety. Di-hydroxylation of TD is

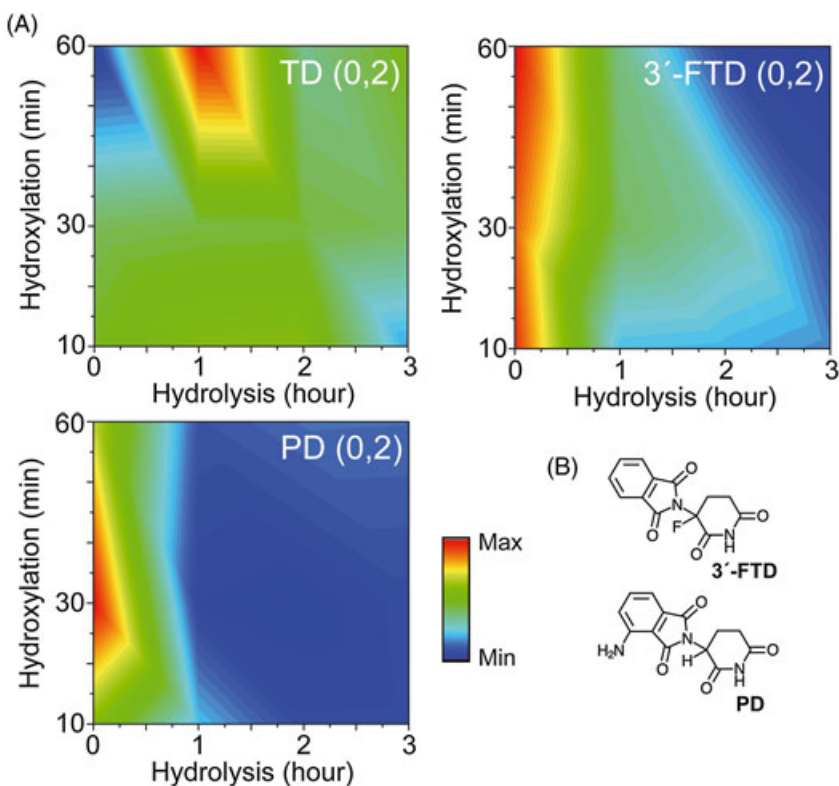


FIGURE 4 (A) Level plots of the amount of (0,2)-metabolites of TD, 3'-FTD, and PD with different hydrolysis and hydroxylation reaction times. The amounts of metabolites were normalized to the maximum amount of each metabolite. (B) Structure of 3'-FTD and PD.

completed with further electron transfer and transformation to the keto-form (Figure S5). The extra hydrolysis time may contribute to this nonenzymatic oxidation, which results in the di-hydroxylated metabolites of TD. On the TD derivatives, this nonenzymatic oxidation of monohydroxylated molecules may be promoted by the disturbance of the electron density induced by a substituent with a fluorine atom or amino moiety.

3.4 | Conservation of chirality in hydrolyzed and hydroxylated metabolites

The above LC–MS/MS assays with a normal reverse phase column did not detect the chirality of the samples. To reveal the change in the chirality of the generated metabolites during hydrolysis and hydroxylation, we measured absorbance and CD spectra of the reaction solutions for different metabolic reaction times. Figure 5 demonstrates the time dependence of the absorbance and CD spectra of the reaction solutions. As TD hydrolysis was under way, the CD signal around 250 nm became gradually smaller and then disappeared, which was originated from ring opening and racemization of TD (Figure 5A). For the reaction solution in the absence of (*S*)-TD, the obvious CD signals were not observed around the wavelength region where the TD metabolites seem to exhibit the CD signals (Figure 5B). This result implies that the proteins and other compounds involved in the reaction solutions do not interrupt the CD signals of the metabolites.

The CD signal around 235 nm remained positive during metabolism, implying that the metabolites that are stable against chiral inversion are generated and conserved in the solution (Figure 5A). The result of theoretical rotatory oscillators and frequency intensities of the (*S*)-isomer of 5-OH-TD show similar signs and intensities compared with the experimental spectra (Figure 5B).

We also computed theoretical absorbance and CD spectra of the most abundant TD metabolites with the same steric configuration, including (*S*)-isomers of *cis/trans*-5'-OH-TD, 5-OH-CBG, and *cis/trans*-5'-OH-TD (Figure S6, S7). The broad absorption band observed in the experiment may be the result of hydroxylated CBG, especially 5-OH-CBG. The summation of the absorbance spectra of the most abundant metabolites and that of the CD spectra agrees with the experimental data (Figure S8), indicating that the chirality of the unmetabolized TD is conserved in the metabolites during the complex metabolic reactions. This also points toward the origin of the enantiospecific efficacy of TD; these metabolites conserve the chirality information, whereas original TD undergoes facile racemization and loses its chirality information.

3.5 | Enantioselectivity in TD metabolic pathway progression

Next, we examined the amounts of some metabolites generated from (*R*)- and (*S*)-TD to determine whether metabolic

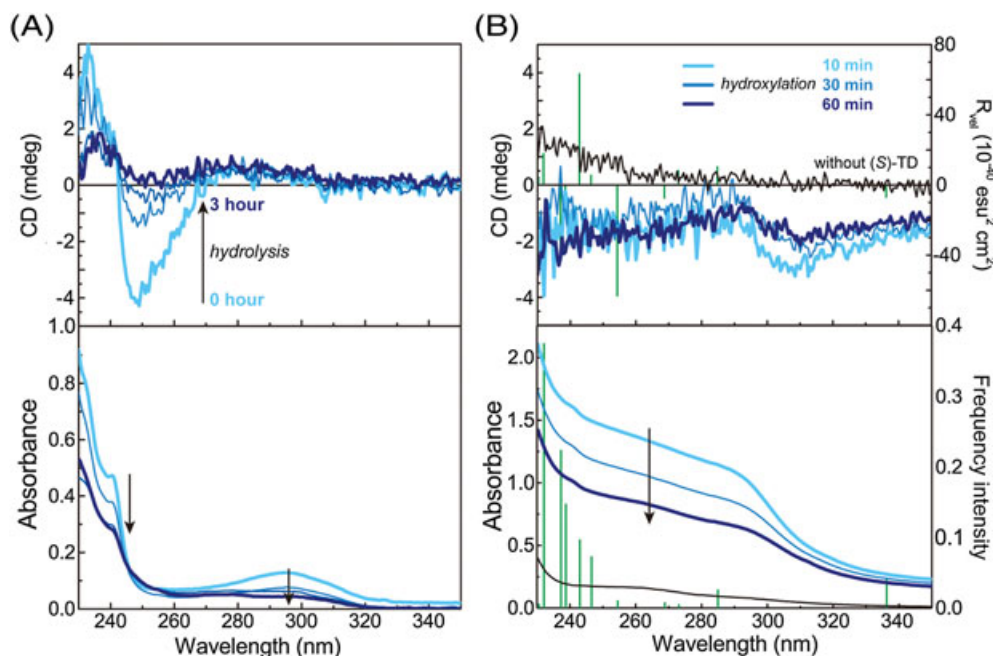


FIGURE 5 (A) Time-dependent changes in absorbance and CD spectra of the sample solutions of (*S*)-TD with 1–3 h of hydrolysis. The light blue and dark blue bold lines represent the absorbance and CD spectra of unmetabolized (*S*)-TD and (*S*)-TD after 3 h of hydrolysis, respectively. (B) Time-dependent changes in absorbance and CD spectra of the sample solutions of (*S*)-TD with 10–60 min of hydroxylation. The light blue and dark blue bold lines represent the absorbance and CD spectra of (*S*)-TD after 10 min and 60 min of hydroxylation, respectively. The green bars show theoretical oscillator strength and rotatory strength of (*S*)-5-OH-TD, one of (0,1)-metabolites of TD

reaction enantioselectivity occurs in the complex TD metabolic systems (Figure 6). We selected (0,0)-, (1,0)- and (1,1)-metabolites for this measurement since these are the dominant metabolites during the metabolic reactions. Moreover, we treated TD for 1 h each of hydrolysis and hydroxylation to allow sufficient time for TD to undergo the metabolic reactions. Obvious differences in the amount

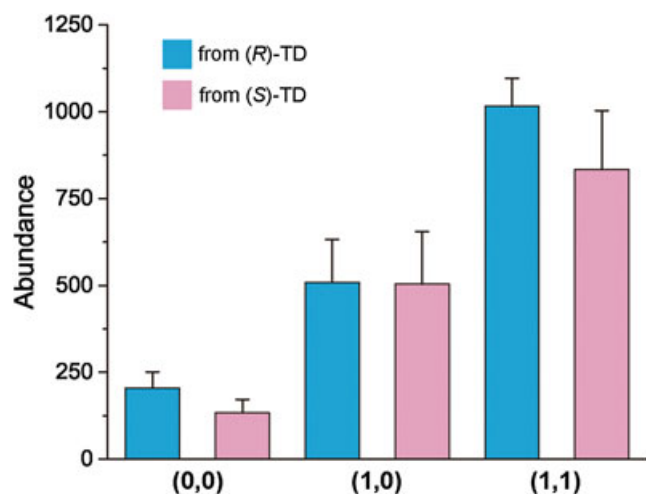


FIGURE 6 Amounts of (0,0)-, (1,0)-, and (1,1)-metabolites generated from (*R*)-TD (blue bars) and (*S*)-TD (red bars) with 1 h of hydrolysis and 60 min of hydroxylation. The values represent mean value ($n = 4$) \pm standard deviation

of these three metabolites generated from different enantiomers of TD were not observed. Therefore, we conclude that there is no enantioselectivity in the metabolic systems of TD. Meyring et al. reported that TD oxidation occurs enantioselectively and that (*R*)-TD preferentially undergoes C-5' oxidation, whereas the opposite enantiomer of TD mainly suffers from C-5 oxidation.⁴² In this study, we did not discriminate between the oxidation sites of TD during LC-MS/MS analysis and regarded all (0,1)-metabolites as the same metabolic step. Thus, our results showed no enantioselectivity in the metabolic reactions of TD. Moreover, these results imply that the combination rates of (*R*)- and (*S*)-TD with P450 would be almost the same even though the binding conformations and the oxidation sites are different between two enantiomers.

3.6 | Activation energy of the first hydrolysis step of TD and its hydroxylated metabolites

To consider the preferential metabolic pathway, we calculated the energy barriers of the first hydrolysis step because these reactions determine the general direction of dynamical metabolic reactions of TD. Figure S9 illustrates the estimated energy diagrams of hydrolysis of TD, 5-OH-TD, and *cis/trans*-5'-OH-TD into CBG, 5-OH-CBG, and *cis/trans*-5'-OH-CBG, respectively. We focused hydrolysis into CBG and hydroxylated CBG since CBG, one of the three

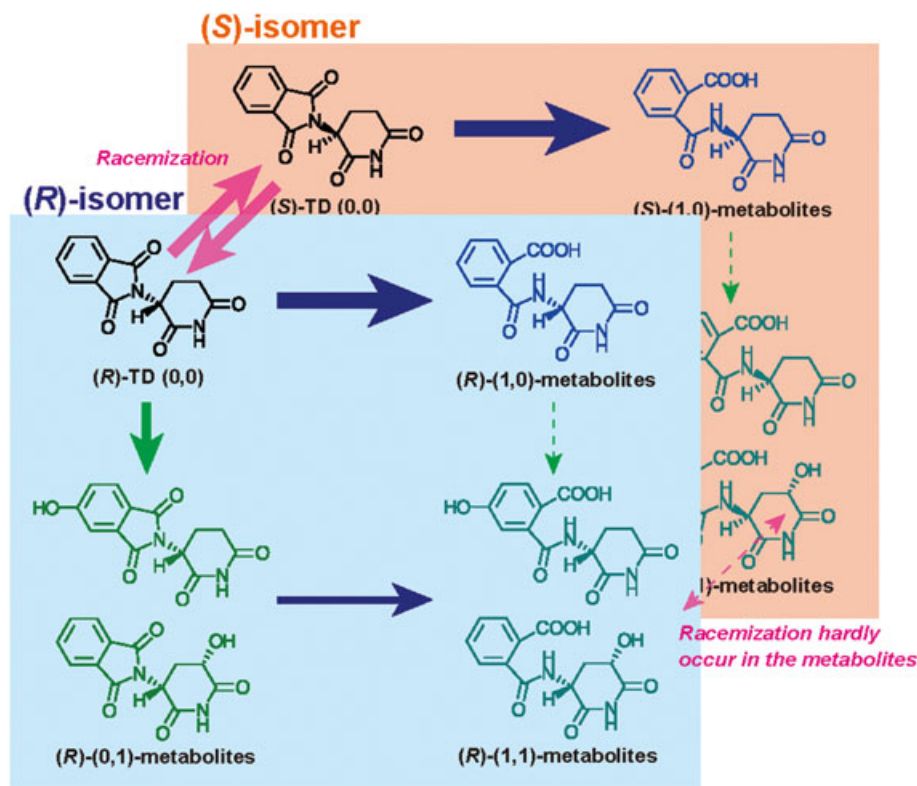


FIGURE 7 Schematic of the preferred pathway for the generation of (1,1)-metabolites involving hydrolysis of TD, hydroxylation of TD, racemization of TD, hydroxylation of (1,0)-metabolites, and hydrolysis of (0,1)-metabolites

(1,0)-metabolites of TD, is preferably generated. In the chiral inversion reaction of TD, two water molecules are involved in deprotonation of the steric center of TD and contribute to the energy barrier decrease for chiral inversion compared with the reaction in an isolated system.⁴³ Our calculation suggests that the hydrolysis reaction involving one water molecule causes a nucleophilic attack on the phthalimide ring and single TS during reaction. Briefly, oxidation at C-5 and C-5' in TD results in an increase in the ring opening energy barrier about 17–18 kcal mol⁻¹ compared with the case of unmetabolized TD. Although the substitution of the hydroxyl moiety on the glutarimide ring causes only slight changes in the molecular structure, oxidation at C-5 on glutarimide ring or C-5' on the glutarimide ring greatly affected the energy barrier for hydrolysis.

3.7 | Preferred pathway among multiple chiral inversion, hydrolysis, and hydroxylation

The theoretical results shown in Figure S9 agree with the previous experimental results,⁴² but also seem to be inconsistent with our experimental results mentioned above. Our results suggest that (1,1)-metabolites are generated via TD oxidation followed by ring breakdown of (0,1)-metabolite. Conversely, our theoretical results indicate that hydrolysis of (0,1)-metabolites is energetically unfavorable. This contradictory result can be reasonably explained with the tradeoff relationship among hydrolysis and hydroxylation of TD and metabolites. Hydrolysis of (0,1)-metabolites seems to be unfavorable, but oxidation of ring-breakdown product (1,0)-metabolites are expected to be even more unfavorable since the structural changes via ring opening substantially affect the intermolecular flexibility, which results in the loss of accessibility to P450. Thus, we can conclude again that oxidation occurring first and degradation occurring second is a possible preferable pathway in the generation of (1,1)-metabolites (Figure 7). According to the results shown in Figure 5, chirality of unmetabolized TD is conserved during the metabolic reactions due to the stability to chiral inversion of the metabolites. Furthermore, our results presented in Figure 6 demonstrate that the series of metabolic reactions proceed in almost the same manner between two enantiomers. Therefore, we infer that the chirality balance in the TD metabolites should be determined by the rate constant for racemization of unmetabolized TD, and the manner of subsequent metabolic reactions is likely to be almost independent of each other between two enantiomers (Figure 7). Although the molecular behaviors relevant to chiral inversion of TD derivatives and their metabolites remain unclear, our scheme of the metabolic reaction procedures also allows a simple estimation of chirality balance in the metabolites of TD and its derivatives by considering first-order racemization of TD and its derivatives.

4 | CONCLUSION

We studied the metabolic reaction network of TD and its derivatives using LC–MS/MS, chiroptical spectroscopy, and theoretical computations. The temporal changes in the amount of each metabolite generated with different reaction times revealed that the three types of biotransformation occurring in TD and its derivatives are related. The substitution of the hydrogen atom with a fluorine atom at the stereogenic center and substitution of the amino moiety on the phthalimide ring accelerated hydrolysis and may also accelerate di-hydroxylation via nonenzymatic hydroxylation. We found the preferred pathway in the generation of (1,1)-metabolites, where TD was first oxidized at C-5' on the glutarimide ring, followed by the degradation of (0,1)-metabolites into (1,1)-metabolites. We also found no enantioselectivity in the progress of the metabolic reactions of TD. The chirality of the various metabolites of TD was confirmed to be almost the same as that of unmetabolized TD. Theoretical calculation results of energy barriers demonstrated that oxidation at C-5 or C-5' caused the increase in the hydrolysis energy barriers. The results obtained in the present study will enable us to comprehend the complex metabolic network of TD and its derivatives, as well as to reveal undiscovered drug efficacies of various metabolites of TD and its derivatives when combined with biological studies.

ACKNOWLEDGMENTS

The authors thank Hideko Koshima and Bart Kahr for fruitful discussions and comments on the article. The authors also thank Hiromi Sunaga for technical support on using the analytical apparatus. The present study was supported by JSPS KAKENHI Grant No. 14 J07106 from MEXT, Japan.

REFERENCES

1. Denny WA. Prodrug strategies in cancer therapy. *Eur J Med Chem.* 2001;36:577-595.
2. Testa B. Prodrug research: Futile or fertile? *Biochem Pharmacol.* 2004;68:2097-2106.
3. Kratz F, Müller IA, Ryppa C, Warnecke A. Prodrug strategies in anticancer chemotherapy. *ChemMedChem.* 2008;3:20-53.
4. Ekins S, Mestres J, Testa B. In silico pharmacology for drug discovery: Methods for virtual ligand screening and profiling. *Br J Pharmacol.* 2007;152:9-20.
5. Ekins S, Mestres J, Testa B. In silico pharmacology for drug discovery: Applications to targets and beyond. *Br J Pharmacol.* 2007;152:21-37.
6. Liu Z, Fang H, Reagan K, et al. In silico drug repositioning—what we need to know. *Drug Discov Today.* 2013;18:110-115.
7. Domenici E, Bertucci C, Salvadori P, Wainer IW. Use of a human serum albumin-based high-performance liquid chromatography

- chiral stationary phase for the investigation of protein binding: Detection of the allosteric interaction between warfarin and benzodiazepine binding sites. *J Pharm Sci.* 1991;80:164-166.
8. Kang XF, Cheley S, Guan X, Bayley H. Stochastic detection of enantiomers. *J Am Chem Soc.* 2006;128:10684-10685.
9. Boersma A, Bayley H. Continuous stochastic detection of amino acid enantiomers with a protein nanopore. *Angew Chem Int Ed.* 2012;51:9606-9609.
10. Blaschke G, Kraft HP, Fickentscher K, Kohler F. Chromatographische Racemattrennung von Thalidomid und teratogene Wirkung der Enantiomere. *Arzneim-forsch.* 1979;29:1640
11. Nishimura K, Hashimoto Y, Iwasaki S. (*S*)-form of α -methyl-N(α)-phthalimidoglutarimide, but not its (*R*)-form, enhanced phorbol ester-induced tumor necrosis factor- α production by human leukemia cell HL-60: Implication of optical resolution of thalidomid effects. *Chem Pharm Bull.* 1994;42:1157-1159.
12. Knoche B, Blaschke G. Investigations on the in vitro racemization of thalidomide by high-performance liquid chromatography. *J Chromatogr A.* 1994;666:235-240.
13. Schumacher H, Smith RL, Williams RT. The metabolism of thalidomide: The spontaneous hydrolysis of thalidomide in solution. *Br J Pharmacol.* 1965;25:324-337.
14. Nakamura T, Nogichi T, Miyachi H, Hashimoto Y. Hydrolyzed metabolites of thalidomide: Synthesis and TNF- α production-inhibitory activity. *Chem Pharm Bull.* 2007;55:651-654.
15. Stephens TD, Bunde CJW, Fillmode BJ. Mechanism of action in thalidomide teratogenesis. *Biochem Pharmacol.* 2000;59:1489-1499.
16. Ando Y, Price DK, Dahut WL, Cox MC, Reed E, Figg WD. Pharmacogenetic associations of CYP2C19 genotype with in vivo metabolisms and pharmacological effects of thalidomide. *Cancer Biol Ther.* 2002;1:669-673.
17. Ando Y, Fuse E, Figg WD. Thalidomide metabolism by the CYP2C subfamily. *Clin Cancer Res.* 2002;8:1964-1973.
18. Lu J, Helsby N, Palmer BD, et al. Metabolism of thalidomide in liver microsomes of mice, rabbits, and humans. *J Pharm Exp Ther.* 2004;310:571-577.
19. Nakamura T, Nogichi T, Kobayashi H, Miyachi H, Hashimoto Y. Mono- and dihydroxylated metabolites of thalidomide: Synthesis and TNF- α production-inhibitory activity. *Chem Pharm Bull.* 2006;54:1709-1714.
20. Chowdhury G, Murayama N, Okada Y, et al. Human liver microsomal cytochrome P450 3A enzymes involved in thalidomide 5-hydroxylation and formation of a glutathione conjugate. *Chem Res Toxicol.* 2010;23:1018-1024.
21. Yamazaki H, Suemizu H, Igaya S, et al. In vivo formation of a glutathione conjugate derived from thalidomide in humanized uPA-NOG mice. *Chem Res Toxicol.* 2011;24:287-289.
22. Chowdhury G, Shibata N, Yamazaki H, Guengerich FP. Human cytochrome P450 oxidation of 5-hydroxythalidomide and pomalidomide, an amino analogue of thalidomide. *Chem Res Toxicol.* 2014;27:147-156.
23. Maeno M, Tokunaga E, Yamamoto T, et al. Self-disproportionation of enantiomers of thalidomide and its fluorinated analogue via gravity-driven achiral chromatography: Mechanistic rationale and implications. *Chem Sci.* 2015;6:1043-1048.
24. Soloshonok VA. Remarkable amplification of the self-disproportionation of enantiomers on achiral-phase chromatography columns. *Angew Chem.* 2006;118:780-783.
25. Ito T, Ando H, Suzuki T, et al. Identification of a primary target of thalidomide teratogenicity. *Science.* 2010;327:1345-1350.
26. Lopez-Girona A, Mendy D, Ito T, et al. Cereblon is a direct protein target for immunomodulatory and antiproliferative activities of lenalidomide and pomalidomide. *Leukemia.* 2012;26:2326-2335.
27. Lu G, Middleton RE, Sun H, et al. The myeloma drug lenalidomide promotes the cereblon-dependent destruction of Ikaros proteins. *Science.* 2014;343:305-309.
28. Fischer ES, Böhm K, Lydeard JR, et al. Structure of the DDB1-CRBN E3 ubiquitin ligase in complex with thalidomide. *Nature.* 2014;512:49-53.
29. Chamberlain PP, Lopez-Girona A, Miller K, et al. Structure of the human cereblon-DDB1-lenalidomide complex reveals basis for responsiveness to thalidomide analogs. *Nat Struct Mol Biol.* 2014;21:803-809.
30. Takeuchi Y, Shiragami T, Kimura K, Suzuki E, Shibata N. (*R*)- and (*S*)-3-fluorothalidomides: Isosteric analogues of thalidomide. *Org. Lett.* 1999;1:1571-1573.
31. Yamamoto T, Suzuki Y, Ito E, Tokunaga E, Shibata N. Asymmetric synthesis of both mirror images of 3'-fluorothalidomide by enantiodivergent fluorination using a single, cinchona alkaloid. *Org Lett.* 2011;13:470-473.
32. Lee CJ, Shibata N, Wiley MJ, Wells PG. Fluorothalidomide: A characterization of maternal and developmental toxicity in rabbits and mice. *Toxicol Sci.* 2011;122:157-169.
33. Kumar S, Rajkumar V. Thalidomide and lenalidomide in the treatment of multiple myeloma. *Eur J Cancer.* 2006;42:1612-1622.
34. Kumar G, Lau H, Laskin O. Lenalidomide: In vitro evaluation of the metabolism and assessment of cytochrome P450 inhibition and induction. *Cancer Chemother Pharmacol.* 2009;63:1171-1175.
35. Chen N, Wen L, Lau H, Surapaneni S, Kumar G. Pharmacokinetics, metabolism and excretion of [14 C]-lenalidomide following oral administration in healthy male subjects. *Cancer Chemother Pharmacol.* 2012;69:789-797.
36. Hoffman M, Kasserra C, Reyes J, et al. Absorption, metabolism and excretion of [14 C] pomalidomide in humans following oral administration. *Cancer Chemother Pharmacol.* 2013;71:489-501.
37. Li Y, Zhou S, Hoffmann M, Kumar G, Palmisano M. Modeling and simulation to probe the pharmacokinetic disposition of pomalidomide R- and S-enantiomers. *J Pharmacol Exp Ther.* 2014;350:256-272.
38. Ogino Y, Asahi T. Model of complex chiral drug metabolic systems and numerical simulation of the remaining chirality toward analysis of dynamical pharmacological activity. *J Theor Biol.* 2015;373:117-131.
39. Frisch MJ, Trucks GW, Schlegel HB, et al. *Gaussian 09, Revision D.01.* Wallingford CT: Gaussian, Inc.; 2009.

40. Otagawa K, Ishikawa K, Shiro M, Asahi T. Crystal structure of (*S*)-4-carbamoyl-4-(1,3-dioxo-isindolin-2-yl)butanoic acid. *Acta Crystallogr E*. 2015;71:107-109.
41. Yamamoto T, Shibata N, Sukeguchi D, et al. Synthesis, configurational stability and stereochemical biological evaluations of (*S*)- and (*R*)-5-hydroxythalidomides. *Bioorg Med Chem Lett*. 2009;19:3973-3976.
42. Meyring M, Muhlbacher J, Messer K, et al. In vitro biotransformation of (*R*)- and (*S*)-thalidomide: Application of circular dichroism spectroscopy to the stereochemical characterization of the hydroxylated metabolites. *Anal Chem*. 2002;74:3726-3735.
43. Tian C, Xiu P, Meng Y, Zhao W, Wang Z, Zhou R. Enantiomerization mechanism of thalidomide and the role of water and hydroxide ions. *Chem A Eur J*. 2012;18:14305-14313.

Supporting Information

Additional Supporting Information may be found online in the supporting information tab for this article.

How to cite this article: Ogino Y, Tanaka M, Shimozawa T, Asahi T. LC-MS/MS and chiroptical spectroscopic analyses of multidimensional metabolic systems of chiral thalidomide and its derivatives. *Chirality*. 2017. <https://doi.org/10.1002/chir.22683>